THE JOURNAL OF PHYSICAL CHEMISTRY B

Article

pubs.acs.org/JPCB

Homopolymer Self-Assembly into Stable Nanoparticles: Concerted Action of Hydrophobic Association and Hydrogen Bonding in Thermoresponsive Poly(alkylacrylic acid)s

Marián Sedlák*

Institute of Experimental Physics, Slovak Academy of Sciences, Watsonova 47, 040 01 Košice, Slovakia

ABSTRACT: A new approach to polymer self-assembly was presented recently [M. Sedlák, Č. Koňák, J. Dybal, *Macromolecules* **2009**, *2*, 7430−7438 and 7439−7446.][1,2] where stable polymeric nanoparticles were formed from poly(ethylacrylic acid) homopolymers without any assembly triggering additives, simply by heating polymer solution under conditions of thermosensitivity to certain temperature. In the current Article, we present successful results on poly(propylacrylic acid), which is a more hydrophobic polymer. We also present results on a less hydrophobic polymer from this series, poly(methacrylic acid), from which nanoparticles cannot be formed. Comparison of results on all three polymers gives a solid physicochemical insight and supports the molecular mechanism of the self-assembly previously suggested: The solvent quality gradually worsens upon heating of a thermosensitive polymer solution, and polymer−polymer contacts are preferred over polymer−solvent contacts, which leads to the formation of polymer assemblies. The presence of a significant amount of charge on chains prevents macroscopic phase separation. Upon subsequent cooling to laboratory temperature, the assemblies (nanoparticles) should eventually dissolve; however, this is not the case due to the fact that polymer chains brought to a close proximity at elevated temperatures become hydrogen-bonded. In addition, hydrogen bonds strengthen upon cooling. Mainly carboxylic-carboxylate hydrogen bonds (COOH···COO$^-$) are responsible for the irreversibility of the process and the stability of nanoparticles. Conclusions are supported by results from static and dynamic light scattering, FTIR spectroscopy, and cryo-TEM microscopy. Size of nanoparticles can be monitored during the growth and custom-tailored by tuning critical parameters, especially the degree of ionization, temperature, and time of heating. Nanoparticles are stable over long periods of time. They are stable in a broad range of salt concentrations, including physiological conditions, and possess a mild acceptable degree of polydispersity.

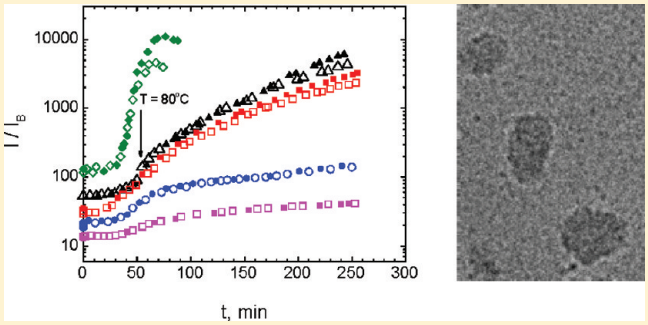

INTRODUCTION

Polymeric nanoparticles are of interest due to numerous existing or foreseen applications. There are many approaches to their formation, which can be divided into chemical (chemical reactions leading to covalent bonds, e.g., latexes, microgels) and physical (self-assembly by physical forces). Physical approaches can be further divided based on the whole variety of mechanisms, for example, copolymer self-assembly in selective solvents (hydrophobic interaction of less soluble blocks),[3−6] association of ionic homopolymers with opposite charges due to electrostatic attraction,[7−10] association of two or more types of homopolymers due to intermolecular hydrogen bonding,[11−14] association of (co)polymers triggered by surfactants,[15,16] termination of the homopolymer phase separation by surfactants which stabilize the system in a dispersed state,[17,18] and so on.

A new approach to polymer self-assembly into stable nanoparticles was presented in our recent work.[1,2] Stable polymeric nanoparticles were prepared from homopolymers (i.e., not copolymers), of one type only (poly(ethacrylic acid)) and without any assembly triggering additives. The self-assembly was based on heating of a thermosensitive poly(ethylacrylic acid) (PEA) solution. Two distinct features were observed, which in consequence have led to a successful preparation of nanoparticles: (i) no macroscopic phase separation was observed, that is, the association ended on a mesoscopic level, and (ii) this association was fully irreversible. The irreversibility was presumably achieved such that chains getting into a close proximity became hydrogen-bonded. As a result, nanoparticles did not dissolve upon cooling to ambient temperature and remained stable. The irreversibility was ascribed mainly to carboxylic-carboxylate hydrogen bonds (COOH···COO$^-$), which are stronger than carboxylic-carboxylic hydrogen bonds of the type COOH···COOH, as shown by model quantum chemical calculations for concrete polymer.[2] Signatures of carboxylic-carboxylate hydrogen bonds were also found experimentally in FTIR spectra.[2] The absence of macroscopic phase separation was ascribed mainly to the

Received: September 1, 2011
Revised: January 24, 2012
Published: January 26, 2012

dx.doi.org/10.1021/jp208445p | *J. Phys. Chem. B* 2012, 116, 2356−2364

ionic character of the polymer, leading to a substantial surface charge of growing associates, as determined also experimentally by electrophoretic light scattering.[1,2]

In the current Article, we present successful results on the preparation of nanoparticles from poly(propylacrylic acid) (PPA), which is a more hydrophobic polymer. We also present results on a less hydrophobic polymer from this series, poly(methacrylic acid) (PMA) and show that nanoparticles cannot be formed from PMA. Comparison of results on all three polymers sheds more light on the nature of the self-assembly process on a molecular level. The important thing is not only the sole difference in hydrophobicity among PMA, PEA, and PPA but mainly the fact that this difference is also reflected in the degree of ionization at which the critical behavior (thermosensitivity) occurs and consequently in the surface charge of growing associates and in the possibility of formation of crucial carboxylic-carboxylate hydrogen bonds.

EXPERIMENTAL SECTION

Material. PPA, M_w = 47 000, M_n = 22 400, M_w/M_n = 2.1, was obtained from Polymer Source, Canada, and used as delivered. PMA, M_w = 70 000, was prepared by radical polymerization. The moisture content in the bulk polymer was established by Karl Fischer method and taken into account in the preparation of exact concentrations. Low molar mass substances were of analytical grade (Merck, Darmstadt). Water was freshly double-distilled in a quartz apparatus and subsequently deionized by analytical grade mixed-bed ion exchange resins (Bio-Rad, Richmond, CA). The resistivity of water was above 15 MΩcm.

Static Light Scattering. The static light scattering (SLS) as well as dynamic light scattering (DLS) measurements were made using a Stabilite 2017-04S argon laser (Spectra Physics, Mountain View, CA) with 514.5 nm vertically polarized beam. Laser power was limited to 100 mW maximum via neutral density filters. A laboratory-made goniometer with angular range from 30 to 150° was used to collect data for both static and DLS experiments. The scattering cell was thermostatted at 25 °C with a precision of ±0.1 °C. All solutions were filtered through 0.2 μm filters. Scattering intensities were measured by photon counting. Solvent scattering was subtracted from total solution scattering to obtain excess scattering intensity. A distilled benzene standard was used for the scattering intensity normalization. Scattering intensities are normalized throughout the work as ratios I/I_B, where I_B is benzene scattering. For the determination of absolute values of molecular weight M_w via a Zimm plot, Rayleigh ratios R_θ were calculated also using a benzene standard. Molecular weight, M_w, of nanoparticles was calculated from a Zimm plot as

$$\lim_{\substack{c\to 0\\ \theta\to 0}} \frac{Kc}{R_\theta} = \frac{1}{M_w} \tag{1}$$

where c is polymer concentration, R_θ is the Rayleigh ratio at scattering angle θ, constant K is defined for vertically polarized incident light as

$$K = \frac{4\pi^2 n^2 (dn/dc)^2}{\lambda_0^4 N_A} \tag{2}$$

where N_A is Avogadro's number, λ_0 is the light wavelength in vacuum, n is solution refractive index, and dn/dc is the refractive index increment. Radius of gyration R_g of nanoparticles can be obtained from the initial slope of the angular dependence at the $c \to 0$ extrapolation

$$\lim_{c\to 0} \frac{Kc}{R_\theta} = \frac{1}{M_w} + \frac{1}{3}\frac{R_g^2}{M_w} q^2 \tag{3}$$

or alternatively from a Guinier plot (plotting log R_θ against q^2), where q is the absolute value of scattering vector $q = (4\pi n/\lambda_0)\sin(\theta/2)$.

Dynamic Light Scattering. An ALV-5000/E correlator with a fast correlation board option (ALV, Langen, Germany) was used for photon correlation measurements. Characteristic decay times of dynamic modes τ_i and their relative amplitudes $A_i(\tau_i)$ were evaluated through the moments of distribution functions of decay times $A(\tau)$ obtained by fitting correlation curves using CONTIN[19] and GENDIST[20,21] programs as

$$g^{(1)}(t) = \int_0^\infty A(\tau) e^{-t/\tau}\, d\tau \tag{4}$$

Diffusion coefficients were calculated as $D_i = (1/\tau_i)q^{-2}$.

Polydispersity index (PDI) reflecting the size polydispersity of nanoparticles was obtained from the cumulant analysis of correlation curves. Fits had the form

$$\ln g^1(t) = \ln A - \bar{\Gamma} t + \frac{\mu_2}{2} t^2 - \frac{\mu_3}{6} t^3 \tag{5}$$

where $g^1(t)$ is the normalized field autocorrelation function, A is amplitude, $\bar{\Gamma}$ is the mean frequency, and μ_2 and μ_3 are the second and the third moments (cumulants), respectively. PDI was calculated as PDI = $\mu_2/\bar{\Gamma}^2$. The physical meaning of PDI can be explained by assuming a Gaussian distribution of sizes R of nanoparticles in the form

$$f(R) = \frac{1}{\sigma\sqrt{2\pi}} \exp\left(-\frac{(R-\bar{R})^2}{2\sigma^2}\right) \tag{6}$$

where σ is the standard deviation $\sigma = (\overline{(R-\bar{R})^2})^{1/2}$. Then, the PDI obtained from the cumulant fit equals PDI = $(\sigma/\bar{R})^2$. The Gaussian distribution has a typical bell shape with the two inflection points at $\bar{R}-\sigma$ and $\bar{R}+\sigma$, respectively. The distribution width characterized as the distance between the two inflection points equals 2σ. This quantity must not be confused with the full width at half-maximum. The "2σ width" corresponds not to the width at 1/2 of the maximum but at 1/1.65 of the maximum and is therefore slightly smaller.

Differential Refractometry. Refractive index increment dn/dc was measured via DNDC-2010 differential refractometer from WGE Dr. Bures (Germany). The 535 nm wavelength was used. Because light scattering was measured at 514.5 nm, the error was negligible. The typical noise level was very small, less than 5×10^{-9} RIU. The main source of error emerging in measuring dn/dc comes from the fact that very rigorously speaking dn/dc of polyelectrolytes or polyelectrolyte nanoparticles should be measured after equilibrium dialysis against solvent. This step is usually skipped in practice because of its time consumption and the problem with a possible change of solution concentration upon dialysis. The resulting error due to omission of equilibrium dialysis depends on the nature of salt used as a supporting electrolyte, more exactly on the nature of the co-ion because the error is due to a negative co-ion adsorption. In the case of NaCl used in this work, the true M_w of nanoparticles may be higher by a few percent than the calculated value based on dn/dc measured without dialysis. The

dx.doi.org/10.1021/jp208445p | J. Phys. Chem. B 2012, 116, 2356−2364

calculation based on semiempirical formulas for linear polyelectrolyte coils[22,23] yields for our polymer charge density and NaCl salt a 10% difference between calculated and true values of M_w, respectively. A smaller difference is anticipated for nanoparticles, which are denser compared with polymer coils.

FTIR Spectroscopy. FTIR spectra were collected on a Thermo Nicolet 6700 advanced gold spectrometer equipped with a DLaTGS detector with KBr window. Samples were measured on a MIRacle ATR unit (Pike) with a Si/ZnSe prism and on a Specac heatable transmission cell GS20513. Spectral resolution was 4 cm^{-1}. ATR spectra were processed by ATR correction.

Cryoelectron Microscopy (cryo-TEM). Samples were vitrified in liquid ethane on holey carbon grids (QUANTIFOIL R 2/2) using a Leica EM GP vitrification robot at 22 °C and 50% humidity. The samples were investigated using a Gatan 626 cryoholder maintained at −180 °C in a FEI Tecnai F20 microscope operated at 200 kV (Electron Microscopy Unit, Institute of Biotechnology, University of Helsinki). The images were recorded with a Gatan US4000 CCD camera at a magnification of 68 000×. Solution was not modified in any way prior to cryo-TEM imaging, neither filtered nor diluted. The darker area with the scalebar corresponds to the carbon grid; the lighter area on the images corresponds to vitrified solution with nanoparticles.

RESULTS AND DISCUSSION

Figures 1 and 2 show comparison of all three polymers under study, PMA, PEA, and PPA, in terms of solution behavior as a function of the degree of neutralization α defined as a ratio of molar concentration of the neutralizing base (NaOH) and monomer molar concentration of the respective polyacid. Plotted are the main parameters extracted from static and DLS data: scattering intensity normalized to benzene scattering I/I_B (Figure 1) and diffusion coefficient D (Figure 2). Both quantities are related to the regular (fast mode) scattering separated from the slow mode scattering from multimacroion domains occurring in polyelectrolyte solutions.[24−28] It is the fast mode behavior that is relevant to the current topic. An increase in scattering intensity is evident upon decreasing α. A moderate increase is observed at higher values of α and is mainly due to increasing osmotic compressibility, in agreement with results of previous works on polycarboxylic acids[1,29,30] as well as theoretical considerations.[31−33] Scattering intensity is then increasing more rapidly at lower values of α and finally diverging at critical α_c corresponding to the phase separation. At lower α, both the polyelectrolyte effect (increased osmotic compressibility) and the influence of approaching the critical behavior (intensity increase by critical fluctuations and/or formation of precritical aggregates) comes into play. However, it is difficult to separate these effects clearly. What is most important for this work is how α_c depends on the nature of the polymer. The stronger the hydrophobic effect (the longer the hydrophobic group in the monomer unit), the higher the α_c. In other words, the stronger the hydrophobic effect, the more charge is necessary to account for polymer solubility. Hence $\alpha_c \cong 0.18$ for PPA, $\alpha_c \cong 0.12$ for PEA, whereas for PMA $\alpha_c = 0$ plus the addition of ∼1.5 M HCl, which suppresses the weak natural ionization occurring at $\alpha = 0$. PEA and PPA solutions were prepared by back-titration because of their relatively weak solubility. Polymer was first dissolved at the degree of neutralization $\alpha = 1.0$ (full neutralization, that is, equal molar concentrations of NaOH and monomer); then, α was decreased gradually via titration by HCl. PMA solutions were prepared directly. The critical conditions for the phase separation of PMA were influenced very little whether prepared directly or indirectly.

The diffusion coefficient (Figure 2) exhibits just opposite behavior to scattering intensity; that is, it decreases with decreasing α and diverges at α_c. This is in agreement with the influence of an electrostatic effect (decreasing of polyion charge causes a slowing down of the coupled diffusion and hence a decrease in the coupled diffusion coefficient) and in agreement with the influence of approaching the critical temperature by lowering α (critical fluctuations or formation of precritical aggregates also slow down diffusion). Another minor effect that comes into play in both the intensity and diffusion coefficient dependencies is that a supporting electrolyte (NaCl) appears in

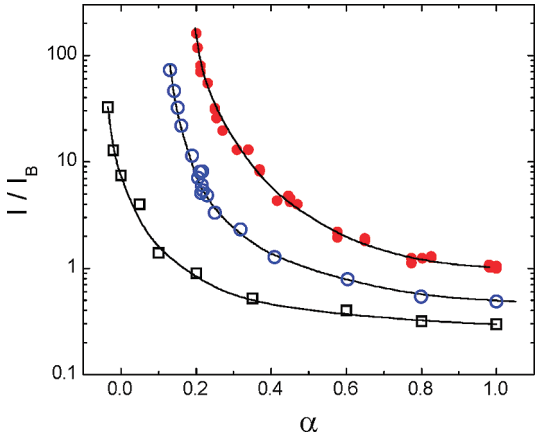

Figure 1. Dependence of scattering intensity on the degree of neutralization α. Solutions of poly(methacrylic acid) (□), poly(ethylacrylic acid) (blue ○), and poly(propylacrylic acid) (red ●) in water partially ionized with NaOH. Polymer concentration c = 20 g/kg. Scattering angle θ = 90°. Intensities shown are excess intensities (solvent contribution subtracted) and are normalized to benzene scattering I_B. Data on poly(ethylacrylic acid) taken from ref 1.

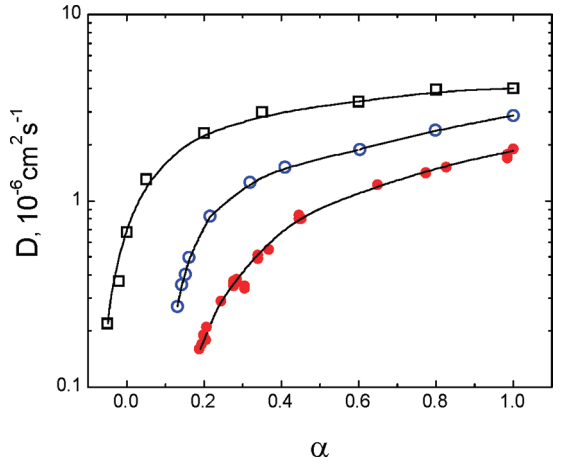

Figure 2. Dependence of diffusion coefficient on the degree of neutralization α. Solutions of poly(methacrylic acid) (□), poly(ethylacrylic acid) (blue ○), and poly(propylacrylic acid) (red ●) in water partially ionized with NaOH. Polymer concentration c = 20 g/kg. Scattering angle θ = 90°. Diffusion coefficient corresponds to the coupled diffusion of polyions and their counterions. Data on poly(ethylacrylic acid) taken from ref 1.

dx.doi.org/10.1021/jp208445p | J. Phys. Chem. B 2012, 116, 2356−2364

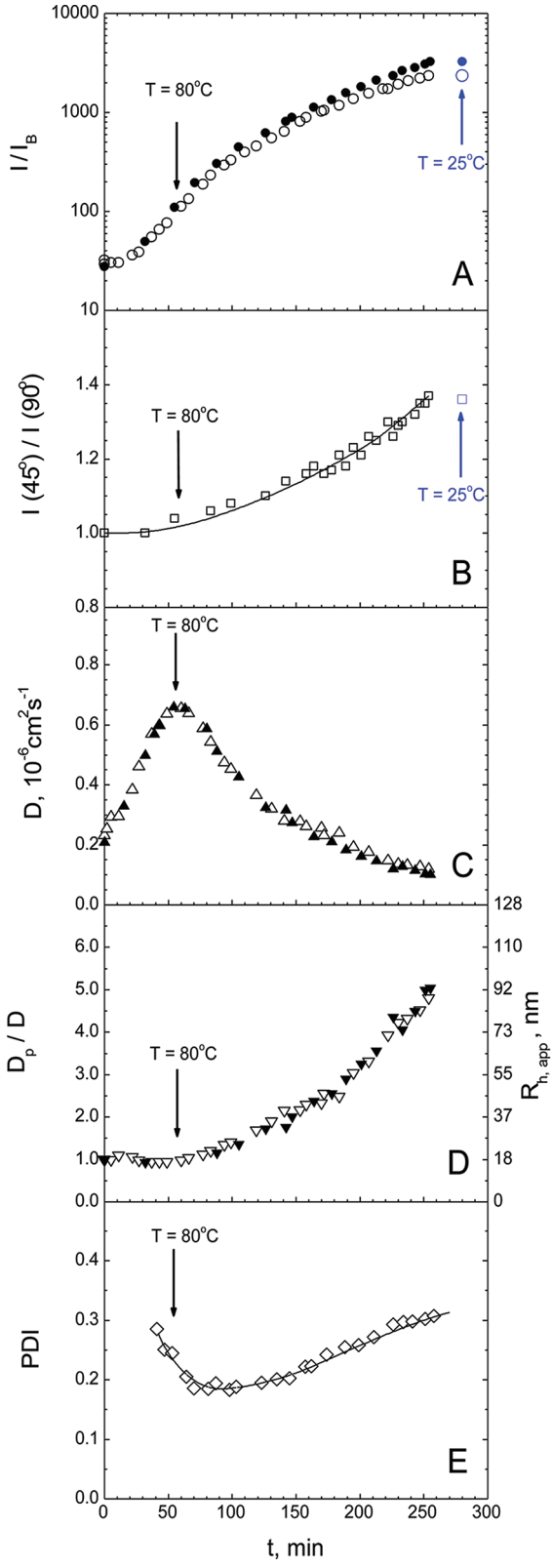

Figure 3. Parameters of light scattering from a PPA solution, α = 0.242, c = 15.7 g/kg, c_s = 130 mM NaCl, during and after heating. Solution was heated from T = 25 to 80 °C at a heating rate 1 °C/min and then kept at 80°C. Scattering angles 90 (open symbols) and 45° (closed symbols), respectively. Scattering after cooling to T = 25 °C is shown by blue symbols. (A) Scattering intensity. (B) Ratio of scattering intensities at 45 and 90°, respectively. (C) Diffusion coefficient. (D) Ratio D_p/D, where D is the actual measured diffusion coefficient at temperature T and D_p is the diffusion coefficient expected at given temperature provided that no change occurs in the sample upon heating except changes of T and solution viscosity η. Increase in D_p/D is due to the increase in the apparent hydrodynamic radius $R_{h,app}$ of nanoparticles. (E) Polydispersity index (PDI) as determined from cumulant analysis.

dx.doi.org/10.1021/jp208445p | J. Phys. Chem. B 2012, 116, 2356–2364

solution upon HCl addition. The effect of increasing salt concentration acts in the same direction as the lowering of polyion charge: increasing scattering intensity and decreasing diffusion coefficient due to shielding of electrostatic interactions and decoupling of polyion and counterion dynamics.[24−27]

It showed up as optimal for nanoparticle preparation from PEA[1,2] to heat a solution back-titrated slightly above α_c, for example, α = 0.21. Now we try the same approach with PPA and then with PMA. Figure 3 shows a summary of data obtained on a process of heat treatment of a PPA solution back-titrated to α = 0.242. It was heated to 80 °C at a rate 1 °C/min and then kept at 80 °C for 3.5 h. Figure 3A shows a dramatic increase in scattering intensity upon heating, which is due to polymer association resulting in particle formation. After cooling to 25 °C the intensity does not drop back but remains constant due to the fact that polymer nanoparticles really do not dissolve but remain stable. Figure 3B shows the ratio of scattering intensities at scattering angles 45 and 90°, $I(45°)/I(90°)$, reflecting the increasing radius of gyration of nanoparticles R_g. Figure 3C shows the diffusion coefficient, which first increases upon heating, then sharply decreases. According to the Stokes−Einstein relation $D = KT/6\pi\eta R_{h,app}$ (K is Boltzmann's constant, T is absolute temperature, η is viscosity, and $R_{h,app}$ is apparent hydrodynamic radius), the initial increase is simply because of the increase in T/η. Then, the nanoparticles start to form, grow in size, and cause a decrease in the diffusion coefficient due to increasing $R_{h,app}$ whereas T/η remains practically constant. An instructional plot is obtained upon correction for the change of T/η (Figure 3D). D_p/D is plotted here, where D is the actual measured diffusion coefficient at a given temperature T (from Figure 3C) and D_p is a "predicted diffusion coefficient" (diffusion coefficient expected at temperature T provided that nothing is changing in the sample upon heating except T and η, $D_p = D_{25}T\eta_{25}/T_{25}\eta$, where D_{25} is the diffusion coefficient measured at 25 °C (the reference temperature), η_{25} is viscosity at 25 °C, and T_{25} = 298 K). The deviation of D_p/D from unity is then a measure of the change of the apparent hydrodynamic radius. The $R_{h,app}$ in Figure 3D is calculated only approximately because the initial $R_{h,app}$ at 25 °C is not known exactly. The development of the PDI with time of heating is shown in Figure 3E. PDI of particle sizes R is defined as PDI = $(\sigma/\bar{R})^2$, where σ is a standard deviation and also a halfwidth of the distribution and was obtained from cumulant analysis of DLS data, as described in detail in the Experimental Section. In the beginning, PDI decreases toward a broad minimum around PDI ≈ 0.18, accompanied by a slow increase in PDI upon further long heating. Smaller nanoparticles (terminated earlier) thus have smaller polydispersity. This is a rather typical behavior observed in aggregation processes.

An exact characterization of resulting nanoparticles was done after cooling and subsequent dilutions. First of all, it is necessary to mention that the nanoparticles are resistant to dilution, that is, that these are stable particles, not some concentration-dependent equilibrium associates.

Molecular weight and the radius of gyration were determined by a Zimm plot. Refractive index increment dn/dc entering the formula for the calculation of molecular weight from the Zimm plot was measured exactly under the conditions at which nanoparticles were formed, that is, degree of neutralization α = 0.242, c = 15.7 g/kg, and c_s= 130 mM NaCl. The hydrodynamic radius was calculated via Stokes−Einstein relation from the zero-angle and zero-concentration extrapolated value of diffusion coefficient D. Solution viscosity η = 0.905 cP determined experimentally at T = 25 °C was used in the calculation. The aggregation number (number of chains involved in a particle) is $N_a \approx 530$. The ratio R_g/R_h = 1.05. Given the uncertainty in the estimate of corresponding radii and the polydispersity complication, we should rather write $R_g/R_h = 1.05 \pm 0.1$. Both R_g and R_h are z-averages; however, $R_{hz} \cong 1/<R_h^{-1}>_z$ whereas $R_{gz} \cong (<R_g^2>_z)^{1/2}$ and therefore large particles are more weighted in R_{gz}. Nevertheless, the value $R_g/R_h = 1.05 \pm 0.1$ is reasonable for polymeric particles (assemblies). We remind that R_g/R_h = 0.778 is the theoretical value for homogeneous spheres and that in practice this ratio can deviate up or down according to the particle density, density distribution inside the particle, as well as draining properties. R_g/R_h values about 1.0 are predicted for random polycondensates (so-called soft balls) and star molecules.[34] R_g/R_h values about 1.0 were also found experimentally for polyelectrolyte complexes.[35] Values clearly below 0.778, which are counterintuitive at first glance, were reported for microgels.[36,37] The apparent structural density ρ of nanoparticles was calculated as an equivalent average density from M_w for the model of a sphere with the radius R_h, with no correction for polydispersity, $\rho = 3M_w/4\pi N_A R_h^3$. The density of PPA nanoparticles described above is smaller than those found for micelles in organic solvents ($\rho \approx 0.2$, see, e.g., ref 38) and for polyelectrolyte complexes (ρ = 0.15 to 0.25, see, e.g., refs 39 and 40) but it is comparable to those found for branched structures.[36] The low density of nanoparticles under investigation is probably due to repulsive interactions between ionized carboxylic groups inside nanoparticles, preventing a more significant compactization. For some applications (e.g., the release of drugs), the low density can be advantageous because the sterical restrictions for a diffusion of low molecular molecules inside of particles are minimized. Regarding PDI, it increases with the time of heating (Figure 3). The sample from Table 1 has PDI = 0.29; smaller particles (terminated earlier) show smaller PDI ≈ 0.15 to 0.2. PDI is thus higher than in the case of micelles[38] (usually smaller than 0.1) while comparable to that of polyelectrolyte complexes, for example, DNA,[40] (0.1 to 0.2). Polydispersity of the most of latexes is above 0.1. Aggregates and microgels are also more polydisperse.

Table 1. Parameters of Nanoparticles Created by the Heating Process Described in Figure 3 Determined by Light Scattering upon Dilution[a]

R_g, nm	R_h, nm	R_g/R_h	M_w, g/mol	dn/dc, mL/g	ρ, g/mL	N_a	PDI
93	89	1.05	2.49×10^7	0.183	0.014	530	0.29

[a]Same values (within experimental accuracy) were obtained after 1 year from the particle preparation. See the text for more details.

SLS and DLS measurements on nanoparticles were repeated after long time intervals (as long as 1 year) with practically identical results. In conclusion, PPA nanoparticles are stable and do not change over long time intervals. Variation of the salt concentration in the range from 0.5 to 600 mM NaCl had no effect on the stability of nanoparticles. This means, of course, also stability at physiological salt concentration.

The effect of the degree of neutralization α on the self-assembly behavior of PPA upon heating is shown in Figures 4 and 5. α is the main parameter by which thermoresponsivity of PPA can be tuned. Figure 4 shows the development of a

dx.doi.org/10.1021/jp208445p | J. Phys. Chem. B 2012, 116, 2356−2364

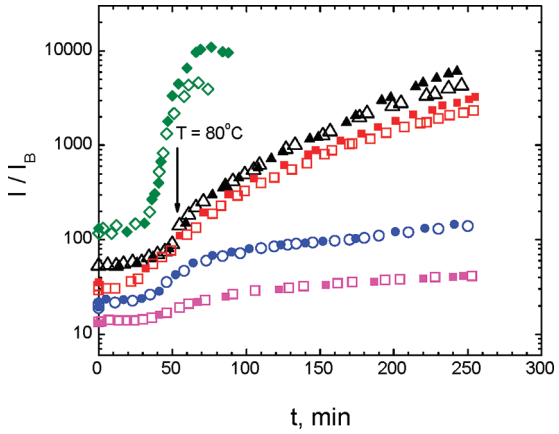

Figure 4. Effect of the degree of neutralization α on the self-assembly behavior of PPA upon heating. Polymer concentration was c = 16 g/kg. Solutions were heated from T = 25 to 80 °C at the heating rate 1 °C/min and then kept at T = 80 °C. Scattering angles 90° (open symbols) and 45° (closed symbols), respectively. α = 0.206 (green ◇), 0.225 (△), 0.242 (red □), 0.285 (blue ○), and 0.304 (pink □). Increase in scattering intensity is due to the irreversible formation of polymeric nanoparticles. Intensities shown are excess intensities (solvent contribution subtracted) and are normalized to benzene scattering I_B.

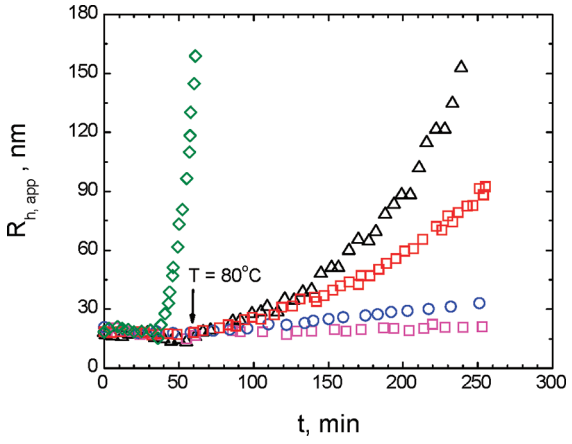

Figure 5. Growth of polymeric nanoparticles upon heating. Dependence on the degree of neutralization α. $R_{h,app}$ is apparent hydrodynamic radius of nanoparticles. Other parameters are the same as in Figure 4.

benzene-normalized scattering intensity, which is proportional to the apparent molecular weight of resulting polymeric nanoparticles. Solutions with higher degrees of neutralization show a weaker effect upon heating because they are more distant from the critical α corresponding to the macroscopic phase separation at ambient temperature (α_{cr}). At α = 0.304, almost no effect is seen upon heating. At the lowest α used (α = 0.206), a very strong and prompt effect was observed, manifested in a very rapid and significant increase in scattering intensity as well as in a large ratio $I(45°)/I(90°)$, both due to arising of rapidly growing large aggregates. Figure 5 shows DLS data. The hydrodynamic radius during heating is calculated only approximately and is denoted as $R_{h,app}$ (apparent). Nevertheless, the DLS data coincide well with the above-described SLS data: the growth of nanoparticles is inversely proportional to the degree of neutralization α.

Behavior of PMA upon heating is significantly different compared with PPA as well as to previously studied PEA.[1,2] Figure 6 shows behavior of moderately charged PMA under conditions where both PEA and PPA form very successfully

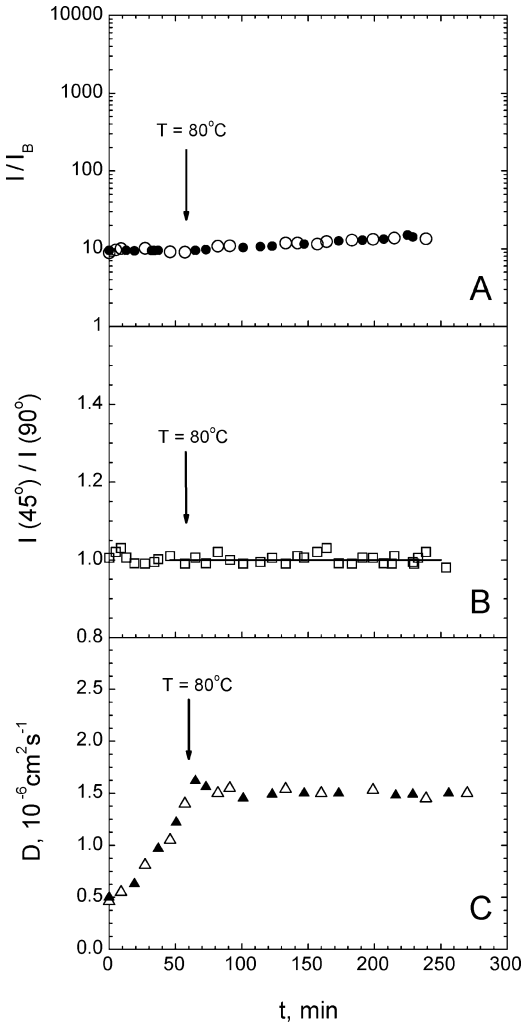

Figure 6. Behavior of a moderately ionized poly(methacrylic acid) solution upon heating from T = 25 to 80°C at the heating rate 1°C/min and then held at 80 °C. α = 0.221, c = 16 g/kg, and c_s = 100 mM NaCl. (A) Scattering intensity at 90° normalized to benzene scattering. (B) Ratio of scattering intensities at 45 and 90°, respectively. (C) Diffusion coefficient.

polymeric nanoparticles (i.e., α = 0.22, c = 16 g/kg, c_s= 100 mM NaCl). Practically no signs of thermosensitivity are seen. Only a very subtle increase in scattering intensity occurs upon heating (Figure 6A), angular ratio is constant (Figure 6B), and diffusion coefficient reflects only a change in KT/η (Figure 6C). This is in agreement with the fact that moderately ionized PMA ($\alpha \approx$ 0.2) is far from the critical conditions (Figures 1 and 2). Hydrophobicity of the methyl group is overcompensated by very hydrophilic ionic carboxylate groups. A different situation is met when the natural ionization of carboxylic groups (occurring spontaneously even in pure water without neutralizing hydroxide) is suppressed by the addition of a strong acid, for example, HCl. Figure 7 shows behavior of PMA in 20 mM DCl. Deuterated version of hydrochloric acid in D_2O was used because of technical reasons (FTIR measurements that will be described later), whereas no difference between the behavior in hydrogenated and deuterated solvent was found.

dx.doi.org/10.1021/jp208445p | J. Phys. Chem. B 2012, 116, 2356–2364

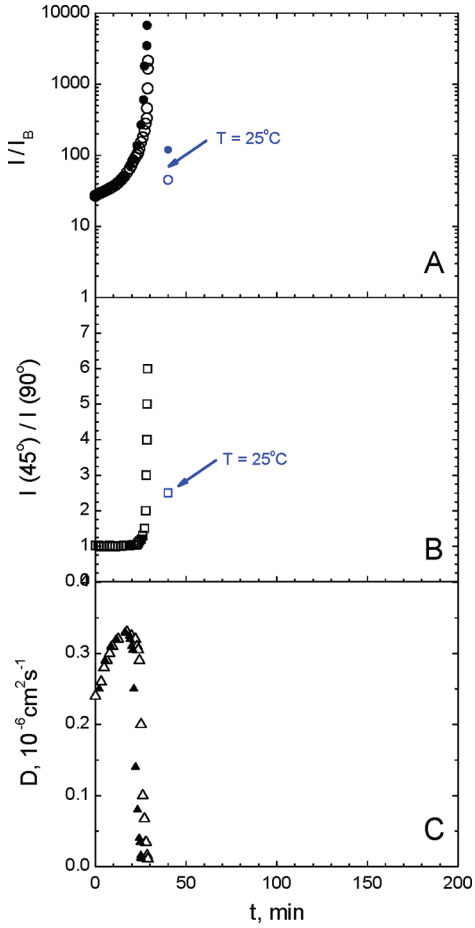

Figure 7. Behavior of a nonionized poly(methacrylic acid) in 20 mM DCl (deuterated hydrochloric acid in D_2O), c = 25 g/kg. Solution was heated at the heating rate 1°C/min. (A) Scattering intensity at 90° normalized to benzene scattering. (B) Ratio of scattering intensities at 45 and 90°, respectively. (C) Diffusion coefficient.

The heating rate was 1 °C/min, similarly to previous experiments. Scattering intensity strongly increases and virtually diverges before reaching 80 °C due to a macroscopic phase separation (Figure 7A). This separation is really macroscopic, not mesoscopic as in the case of heating ionized PEA or PPA. It is seen that the angular dissymmetry increases very dramatically (Figure 7B), whereas diffusion coefficient decreases very dramatically (Figure 7C), both due to the formation of extremely large aggregates followed by a naked eye observable macroscopic phase separation. Another crucial difference is that the transition is reversible in a sense that the macroscopically segregated polymeric material dissolves upon decreasing temperature and solution becomes again homogeneous and optically transparent. However, a very thorough and detailed inspection by light scattering shows that some small traces of large polydisperse aggregates can be found in solution and persist at least weeks after cooling. (See blue symbols in Figure 7 showing that light scattering parameters do not drop exactly back to the original value.) The weight fraction of polymer trapped in these aggregates is, however, very small. It can be concluded that the phase transition is almost fully reversible. As seen from results presented in Figures 6 and 7, PMA is not suitable for the preparation of nanoparticles by the presented method. In both cases of PEA and PPA the thermosensitivity occurs in a regime of relatively strongly charged chains. In the case of PMA, it occurs in a regime of almost uncharged chains.

To shed more light on molecular mechanisms of aggregation/self-assembly of the polyacids investigated, we conducted FTIR measurements in addition to light scattering. To avoid a strong contribution of H_2O to IR spectra in the region where signal from polymer is expected, all measurements were done in D_2O solutions. This substitution has no effect on the polyacid self-assembly, as checked by separate light scattering measurements.

Figure 8 shows FTIR spectra measured on a PPA solution under conditions promoting successful formation of stable

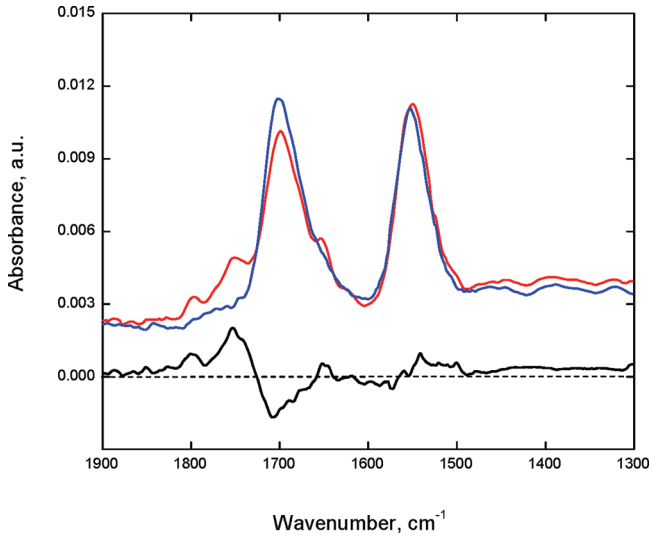

Figure 8. FTIR spectra of PPA, α = 0.228, c = 16 g/kg, and c_s = 135 mM NaCl, prior to heating (blue −) and after heating and cooling according to the usual heating scheme from Figure 3 (red −). Differential spectrum (black −) = spectrum after heating − spectrum before heating. All spectra were acquired in D_2O solutions. Spectrum of D_2O was subtracted.

nanoparticles (α = 0.228, c = 16 g/kg, and c_s = 135 mM NaCl). Spectra were accumulated prior to heating and after heating and cooling according to the usual scheme from Figure 3. The band at 1551 cm^{-1} corresponds to the asymmetric stretching vibrations of carbonyls in the free (non-bonded) COO^- groups, whereas a smaller band at 1400 cm^{-1} corresponds to their symmetric stretching vibrations. Both bands clearly increase with increasing degree of neutralization α, as expected (not shown). The band detected at 1701 cm^{-1} is assigned to the carbonyl stretching vibration in the COOH group hydrogen-bound in the dimer COOH···COOH, eventually hydrated. The intensity of this band decreases after heating, whereas intensity of weak bands at 1752 and 1652 cm^{-1} increases, as can be well seen in the difference spectrum. The appearance of the doublet at 1752 and 1652 cm^{-1} is connected to the emergence of hydrogen bonds COOH···COO^-, and the doublet is assigned to the strongly coupled stretching vibrations of the carbonyls in the COOH and COO^- groups. The appearance of this doublet was also found previously in nanoparticle-forming PEA solutions upon heating, and this assignment was supported by DFT calculations of vibrational frequencies in the hydrogen-bonded structure.[2]

The band at 1797 cm^{-1} is assigned to the carbonyl stretching vibrations of free, non-bonded COOH groups. The free

dx.doi.org/10.1021/jp208445p | J. Phys. Chem. B 2012, 116, 2356−2364

COOH groups are probably buried inside compact structures of PPA nanoparticles, where they cannot form hydrogen bonds due to the sterical hindrance. This is in agreement with the expected polymer compactization upon heating. In conclusion, FTIR measurements suggest that similarly to PEA, the main stabilization forces responsible for the irreversibility of the self-assembly of PPA are hydrogen bonds, especially COOH···-COO^- bonds, which have significantly higher interaction energies compared with COOH···COOH bonds, which was previously also supported by quantum chemical calculations.[2]

Figure 9 shows FTIR results on the moderately ionized PMA sample from Figure 6 (α = 0.221, c = 16 g/kg, and c_s = 100 mM

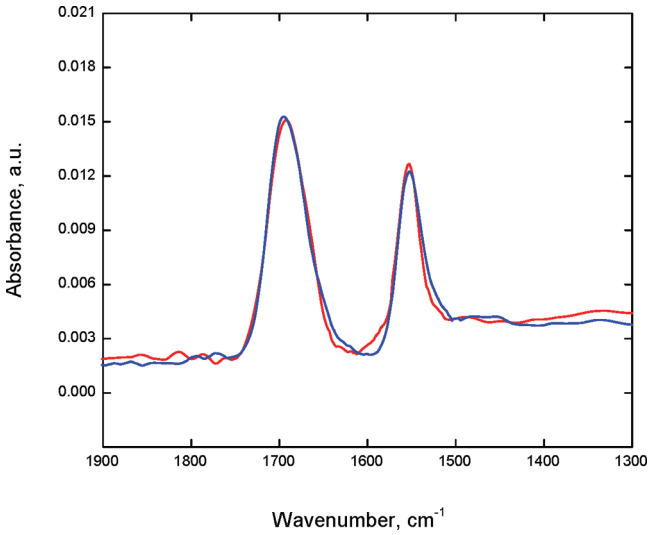

Figure 9. FTIR spectra of PMA, α = 0.221, c = 16 g/kg, c_s = 100 mM NaCl, prior to heating (blue −) and after heating and cooling according to the usual heating scheme from Figure 3 (red −). All spectra were acquired in D_2O solutions. Spectrum of D_2O was subtracted.

NaCl), which showed no ability of nanoparticle formation. Two bands dominate the spectrum here: the band at 1552 cm^{-1} corresponding to the asymmetric stretching vibrations of carbonyls in the free (non-bonded) COO^- groups and the band at 1695 cm^{-1} assigned to the carbonyl stretching vibration in the COOH group hydrogen-bound in the dimer COOH···COOH and/or hydrated. In contrast with the case of nanoparticle-forming PPA and PEA solutions, no changes in spectra are observed upon heating, especially no signatures of the formation of COOH····COO^- hydrogen bonds. FTIR data are thus in agreement with light scattering data and support the interpretation of the mechanism of nanoparticle formation given above.

Figure 10 shows FTIR results on the nonionized PMA sample from Figure 7 (ionization suppressed in 20 mM DCl). The spectrum is dominated by the band at ∼1700 cm^{-1} assigned to the carbonyl stretching vibration in the COOH group hydrogen-bound in the dimer COOH···COOH and/or hydrated, whereas the band at ∼1550 cm^{-1} corresponding to the asymmetric stretching vibrations of the free (non-bonded) COO^- groups is hardly visible just because of the (almost total) suppression of ionization. No change is seen in the spectrum upon heating, in agreement with the fact that this polymer is most probably bound in aggregates by COOH···COOH hydrogen bonds and the carbonyl stretching vibration in the

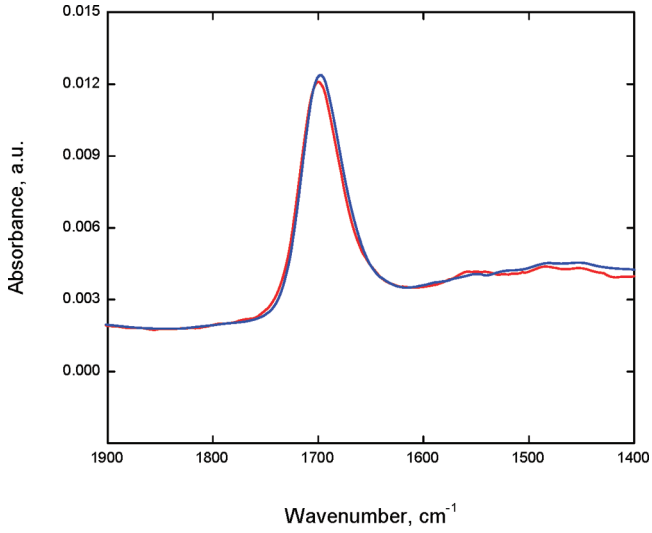

Figure 10. PMA in 20 mM DCl (deuterated hydrochloric acid in D_2O). FTIR spectra measured prior to heating at T = 25°C (blue −) and after heating at T = 60°C (red −). Spectrum of 20 mM DCl in D_2O was subtracted.

COOH groups hydrogen-bound in the dimer COOH···COOH is practically the same as the vibration in hydrated carboxylic groups (both bands at ∼1700 cm^{-1}). We also suppose that the tiny population of aggregates that persists in solution upon completion of a heating cycle does not reflect in FTIR spectra because of the very small weight fraction of polymer in these aggregates.

CONCLUSIONS

A comparison of behavior of three polycarboxylic acids (PMA, PEA, and PPA) studied by SLS, DLS, and FTIR spectroscopy sheds light on molecular mechanisms of polymer aggregation/self-assembly due to worsening of solvent quality by heating (thermosensitive behavior). The situation is different in PMA solutions compared with PEA and PPA solutions. This difference is caused by the fact that the thermoresponsivity of PMA (close to the critical conditions) is achieved in a situation where ionization is almost completely suppressed in acidic environment, and this is further reflected in two effects: (i) lower barrier in aggregation due to missing strong electrostatic repulsion between aggregating chains and (ii) absence of carboxylate groups capable of strong and irreversible hydrogen bonding with carboxylic groups. As a result, PMA undergoes macroscopic (not mesoscopic) phase separation and the process is reversible. In contrast, PEA and PPA achieve thermoresponsivity while relatively strongly charged (ionization 20−25%, which is not very far from the maximum critical ionization of ∼35% at the counterion condensation onset). The presence of an ionized form of polymer results in a mesoscopic phase separation and in full irreversibility due to the formation of carboxylate-carboxylic hydrogen bonds. As a result, stable nanoparticles with discrete dimensions can be formed. The process of their formation can be monitored online by light scattering, and particle size can be custom tuned. Obtained nanoparticles have interesting properties. They are very stable over long periods of time (excellent shelf life) and are stable in a broad range of salt concentrations including physiological conditions. Figure 11 shows representative cryo-TEM images of such nanoparticles. Electron micrographs clearly confirm their

dx.doi.org/10.1021/jp208445p | J. Phys. Chem. B 2012, 116, 2356−2364

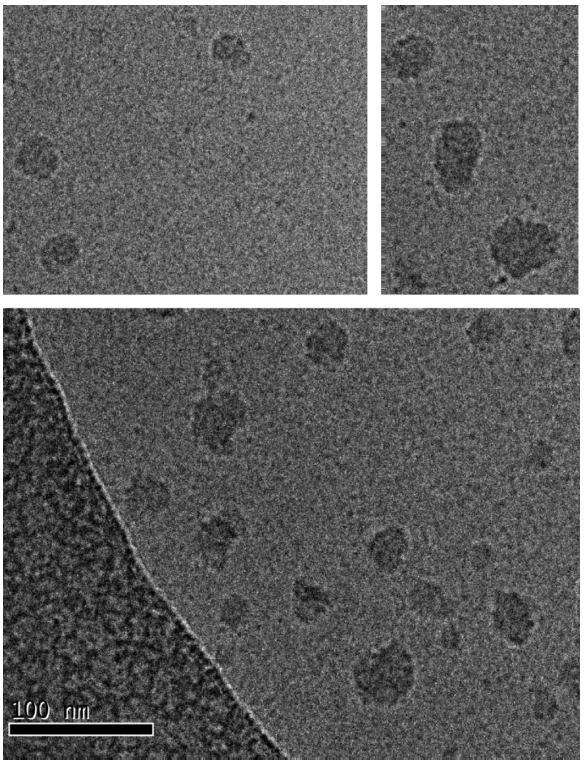

Figure 11. Representative cryogenic transmission electron microscopy micrographs of PEA nanoparticles. Solution of PEA (polymer concentration c = 16 g/kg, degree of neutralization α = 0.22) after temperature cycling T = 25 → 80 → 25 °C. Bar indicates 100 nm.

presence in solution and also provide some additional information not available from light scattering data. Nanoparticles have cobble-like shape and uniform internal density. No indication of a hollow structure with outer shell is found. The formation of irreversible carboxylate-carboxylic hydrogen bonds, as described in this work, has a potential to be applied as a molecular construction tool in other systems and architectures. The work in this direction is already in progress.

AUTHOR INFORMATION

Corresponding Author

*E-mail: marsed@saske.sk.

Notes

The authors declare no competing financial interest.

ACKNOWLEDGMENTS

Support of the Scientific Grant Agency VEGA (grant no. 2/0215/10) and Slovak Research and Development Agency (grant no. 048610) is acknowledged. This work was realized within the frame of the project "Centre of Excellence for Advanced Materials With Nano- and Submicrometer Structure", which is supported by the Operational Program "Research and Development" of the Slovak republic financed through European Regional Development Fund. The author would like to thank K. Vrancová and D. Rak for technical assistance in the realization of some experiments. The author is also thankful to P. Laurinmaki for acquiring cryoelectron microscopy images and to Prof. S. Butcher and the Biocenter Finland National Cryoelectron Microscopy Unit for providing facilities. This paper is dedicated to the memory of Dr. Č. Koňák, Institute of Macromolecular Chemistry, Academy of Sciences of the Czech Republic.

REFERENCES

(1) Sedlák, M.; Koňák, Č. *Macromolecules* **2009**, *42*, 7430−7438.
(2) Sedlák, M.; Koňák, Č.; Dybal, J. *Macromolecules* **2009**, *42*, 7439−7446.
(3) Forster, S.; Antonietti, M. *Adv. Mater.* **1998**, *10*, 195−217.
(4) Allen, C.; Maysinger, D.; Eisenberg, A. *Colloids Surf., B* **1999**, *16*, 3−27.
(5) Riess, G. *Prog. Polym. Sci.* **2003**, *28*, 1107−1170.
(6) Lee, A. S.; Butun, V.; Vamvakaki, M.; Armes, S. P.; Pople, J. A.; Gast, A. P. *Macromolecules* **2002**, *35*, 8540−8551.
(7) Dautzenberg, H. In *Physical Chemistry of Polyelectrolytes*; Radeva, T., Ed.; Marcel Dekker: New York, 2001; Chapter 20.
(8) Mattison, K. W.; Dubin, P. L. *J. Phys. Chem. B* **1998**, *102*, 3830−3836.
(9) Sui, Z. J.; Jaber, J. A.; Schlenoff, J. B. *Macromolecules* **2006**, *39*, 8145−8152.
(10) Schonhoff, M. *J. Phys.: Condens. Matter* **2003**, *15*, 1781−1808.
(11) Juang, M.; Li, M.; Xiang, M.; Zhou, H. *Adv. Polym. Sci.* **1999**, *146*, 121−196.
(12) Poe, G.; Jarrett, W.; Scales, C.; McCormick, C. *Macromolecules* **2004**, *37*, 2603−2612.
(13) Chen, H. L.; Morawetz, H. *Macromolecules* **1982**, *15*, 1445−1447.
(14) Sukhishvili, S. A.; Granick, S. *Macromolecules* **2002**, *35*, 301−310.
(15) Thunemann, A. F. *Prog. Polym. Sci.* **2002**, *27*, 1473−1572.
(16) Makhaeva, E. E.; Tenhu, H.; Khokhlov, A. R. *Macromolecules* **1998**, *31*, 6112−6118.
(17) Koňák, Č.; Hrubý, M. *Macromol. Rapid Commun.* **2006**, *27*, 877.
(18) Koňák, Č.; Pánek, J.; Hrubý, M. *Colloid Polym. Sci.* **2007**, *285*, 1433.
(19) Provencher, S. W. *Comput. Phys. Commun.* **1982**, *27*, 213−227.
(20) Jakeš, J. *Czech. J. Phys.* **1988**, *38*, 1305.
(21) Štěpánek, P. In *Dynamic Light Scattering. The Method and Some Applications* ; Clarendon: Oxford, U.K., 1993; Chapter 4.
(22) Sedlák, M. In *Light Scattering: Principles and Development*; Clarendon Press: Oxford, U.K., 1996; Chapter 4.
(23) Vrij, A.; Overbeek, J.; Th., G. *J. Colloid. Sci.* **1962**, *17*, 570−588.
(24) Lin, S. C.; Lee, W. I.; Schurr, J. M. *Biopolymers* **1978**, *17*, 1041.
(25) Schmitz, K. S. *Macroions in Solution and Colloidal Suspension*; VCH Publishers, New York, 1993.
(26) Sedlák, M. In *Physical Chemistry of Polyelectrolytes*; Marcel Dekker: New York, 2001; Chapter 1.
(27) Sedlák, M. *Langmuir* **1999**, *15*, 4045−4051.
(28) Förster, S.; Schmidt, M.; Antonietti, M. *Polymer* **1990**, *31*, 781−792.
(29) Sedlák, M.; Koňák, Č.; Štěpánek, P.; Jakeš, J. *Polymer* **1987**, *28*, 873−880.
(30) Sedlák, M. *J. Chem. Phys.* **2002**, *116*, 5256−5262.
(31) Manning, G. S. *J. Chem. Phys.* **1969**, *51*, 924.
(32) Kakehashi, R.; Yamazoe, H.; Maeda, H. *Colloid Polym. Sci.* **1998**, *276*, 28−33.
(33) Chang, R.; Yethiraj, A. *Macromolecules* **2005**, *38*, 607−616.
(34) Burchard, W. *Adv. Polym. Sci.* **1983**, *48*, 1.
(35) Oupický, D.; Koňák, Č.; Ulbrich, K. *J. Biomater. Sci., Polymer Ed.* **1999**, *10*, 573.
(36) Schmidt, M. In *Dynamic Light Scattering: The Method and Some Applications*; Clarendon: Oxford, U.K., 1993; Chapter 8.
(37) Burchard, W. In *Light Scattering. Principles and Development*; Clarendon Press: Oxford, U.K., 1996; Chapter 13.
(38) Tuzar, T.; Pleštil, J.; Koňák, Č.; Hlavatá, D.; Sikora, A. *Makromol. Chem.* **1983**, *184*, 2111−2121.
(39) Dautzenberg, H.; Koňák, Č.; Reschel, T.; Zintchenko, A.; Ulbrich, K. *Macromol. Biosci.* **2003**, *3*, 425.
(40) Reschel, T.; Koňák, Č.; Oupický, D.; Seymour, L. W.; Ulbrich, K. *J. Controlled Release* **2002**, *81*, 201.